*Chapter 2*

# Functional characterization of Rho GTPases in *Aspergillus niger* uncovers conserved and diverged roles of Rho-proteins within filamentous fungi

**Min Jin Kwon*, Mark Arentshorst*, Eelke D. Roos, Cees A.M.J.J van den Hondel, Vera Meyer and Arthur F.J. Ram**

*: both authors equally contributed to this work

Mol Microbiol (2011) 79(5):1151-67.

## Abstract

Rho GTPases are signalling molecules regulating morphology and multiple cellular functions including metabolism and vesicular trafficking. To understand the connection between polarized growth and secretion in the industrial model organism *Aspergillus niger*, we investigated the function of all Rho family members in this organism. We identified six Rho GTPases in its genome and used loss-of-function studies to dissect their functions. While RhoA is crucial for polarity establishment and viability, RhoB and RhoD ensure cell wall integrity and septum formation, respectively. RhoC seems to be dispensable for *A. niger*. RacA governs polarity maintenance via controlling actin but not microtubule dynamics, which is consistent with its localization at the hyphal apex. Both deletion and dominant activation of RacA ($Rac^{G18V}$) provoke an actin localization defect and thereby loss of polarized tip extension. Simultaneous deletion of RacA and CftA (Cdc42) is lethal; however, conditional overexpression of RacA in this strain can substitute for CftA, indicating that both proteins concertedly control actin dynamics. We finally identified NoxR as a RacA-specific effector, which however, is not important for apical dominance as reported for *A. nidulans* but for asexual development. Overall, the data show that individual Rho GTPases contribute differently to growth and morphogenesis within filamentous fungi.


## Introduction

Small monomeric GTPases are found in all eukaryotic organisms and function as molecular switches to regulate a vast array of cellular processes including metabolism, survival, morphogenesis, differentiation and vesicle transport. Based on structural similarities, small GTPases are grouped into five subfamilies: Ras, Rho (Ras homolog), Arf/Sar, Ran and Rab/Ypt. The Rho subfamily is the most extensively characterized subfamily and comprises six members in lower eukaryotes (e.g. Rho1p, Rho2p, Rho3p, Rho4p, Rho5p, Cdc42p in the yeast *Saccharomyces cerevisiae*) and more than 20 members in higher eukaryotes, with RhoA, Rac1 and Cdc42 being most studied (Heasman and Ridley 2008; Park and Bi 2007; Ridley 2006). Most Rho GTPases cycle between a GTP-bound (active) and a GDP-bound (inactive) form which is controlled by guanine nucleotide exchange factors (GEFs) and GTPase-activating proteins (GAPs). The localization of Rho GTPases to membranes and membrane compartments is post-transcriptionally regulated by prenylation (farnesylation or geranylgeranylation) of their C-terminus. This lipid modification defines the specificity to and enhances the interaction of Rho GTPases with different membranes. Guanine nucleotide dissociation inhibitors (GDIs) bind to prenyl groups of GTPases thereby

inhibiting their membrane localization as well as preventing their interaction with effector proteins. Thus, the activity of Rho GTPases is not only dependent on a functional GTP/GDP cycle but also on a membrane/cytosol cycle (Casey 1994; Dransart et al. 2005; Ridley 2006).

Various effector pathways have been discovered in eukaryotes which lie downstream of Rho GTPases: i) Actin filament nucleation and (de)polymerization on or close to membranes is regulated by interaction of Rho proteins (e.g. Rho1p/RhoA, Rac1, Cdc42) with WASP proteins, formins and PAK kinases. Because actin dynamics is closely linked to membrane dynamics and vesicular trafficking, the function of Rho GTPases is intimately linked to exocytosis, endocytosis as well as to polarized cell shape changes and cell movement (Bosco et al. 2009; Heasman and Ridley 2008; Park and Bi 2007; Ridley 2001; Ridley 2006). ii) Localized generation of reactive oxygen species (ROS) results from Rac1-mediated activation of NADPH oxidases (note that the hemiascomycetes *S. cerevisiae* and *Schizosaccharomyces pombe* do not comprise a Rac1 homolog). The regulated synthesis of ROS plays a key role in host defense responses and differentiation of multicellular organisms (Hordijk 2006; Scott and Eaton 2008). iii) Activation of cell wall synthesizing enzymes such as β-1,3 glucan synthases in *S. cerevisiae* and *S. pombe* is mediated by Rho1 (Arellano et al. 1996; Qadota et al. 1996) and positive regulation of α-1,3 glucan synthase activities has been shown for the *S. pombe* Rho2 (Calonge et al. 2000). iv) Finally, some Rho proteins have been shown to modulate gene transcription in mammalian cells as for example documented for the transcription factors NFκB, AP1 and c-Jun (Benitah et al. 2004; Schlessinger et al. 2009).

Based on genome mining approaches, six Rho encoding genes have been predicted in filamentous fungi – *rac1*, *cdc42* and four genes encoding putative *S. cerevisiae* homologs of Rho1p, Rho2p, Rho3p, Rho4p (http://www.broadinstitute.org/ and (Banuett et al. 2008; Boureux et al. 2007; Harris et al. 2009; Rasmussen and Glass 2005)). Over the past years, a crucial involvement of some of these Rho GTPases in the orchestration of the highly polarized growth mode of filamentous fungi has become apparent. For example, Rac1 and Cdc42 orthologs have been demonstrated to be pivotal for morphogenetic decisions e.g. in *Aspergillus nidulans*, *Claviceps purpurea*, *Magnaporthe grisea*, *Penicillium marneffi* and *Ustilago maydis* (Boyce et al. 2003; Chen et al. 2008; Mahlert et al. 2006; Rolke and Tudzynski 2008; Virag et al. 2007). Rac1-mediated activation of fungal NADPH oxidases has been shown to generate tip-localized ROS in *A. nidulans* and *Epichloë festucae* which are suspected to be essential for sustaining apical dominance (Scott and Eaton 2008; Semighini and Harris 2008; Takemoto et al. 2006). Rho1 orthologs have been shown to be essential for hyphal tip extension and cell wall biosynthesis in *A. nidulans*, *Ashbya gossypii*, *Fusarium oxysporum* and *U. maydis* (Guest et al. 2004; Martinez-Rocha et al. 2008; Pham

et al. 2009; Wendland and Philippsen 2001). Considerably less information is available on the function of Rho2, Rho3 and Rho4 orthologs in filamentous fungi. An involvement of Rho3 in polar growth control has so far been documented for *A. gossypii* and *Trichoderma reesei* (Vasara et al. 2001; Wendland and Philippsen 2001), and a role of Rho4 for actin ring formation during hyphal septation has been established for *Neurospora crassa* and *A. nidulans* (Rasmussen and Glass 2005; Si et al. 2010).

As part of our effort to understand the connection between the processes of polarized growth, cell wall biosynthesis and secretion in the industrially important fungus *A. niger*, we use genome-wide expression profiling studies to predict and identify signalling molecules and networks involved in these processes (Jacobs et al. 2009; Jørgensen et al. 2009; Meyer et al. 2009; Meyer et al. 2007b). We furthermore implement functional genomics approaches to study the cellular role of predicted protagonist coordinating these processes (Damveld et al. 2005; Meyer et al. 2009; Meyer et al. 2008; Meyer et al. 2010a; Punt et al. 2001). Here, we systematically investigated the function of all members of the Rho family for growth and morphogenesis of *A. niger*. We identified six Rho GTPases in the genome of *A. niger* and used loss-of-function studies which showed that they exert distinct and overlapping functions during the life cycle of *A. niger*. While RhoA appears to be of central importance for polarity establishment and viability of *A. niger*, RhoB and RhoD ensure cell wall integrity. Whereas RhoC seems to be of minor importance for *A. niger*, RhoD has a pivotal role during septum formation. RacA and CftA (Cdc42) collectively ensure polarity maintenance, whereby the main protagonist is RacA. We furthermore show that RacA localizes to the hyphal apex and controls actin dynamics but not microtubule integrity and finally identified two downstream targets of RacA which are not shared with CftA. Most importantly, this work uncovers lack of uniformity in how members of the Rho GTPase family are deployed in filamentous fungi.

# Results

## *A. niger* has six Rho GTPases-encoding genes

Screening of the genome sequence of *A. niger* (Pel et al. 2007) revealed the presence of six open reading frames (ORFs) (An18g05980, An16g04200, An11g09620, An14g05530, An11g10030, An02g14200), each predicted to encode a single member of the Rho subfamily. Phylogenetic comparison with (predicted) Rho GTPases from *A. nidulans, N. crassa, M. grisea, P. marneffei*, *S. cerevisiae, S. pombe* and *U. maydis* showed that each subgroup (Rasmussen and Glass 2005) was represented by a single *A. niger* orthologous

**Table 1**. Expression of predicted Rho GTPase genes in *A. niger* wild-type strain N402.

| Gene | ORF code | Germination[a] | Steady state[b] ($\mu$= 0.16 $h^{-1}$) | Exponential growth phase[c] ($\mu$= 0.24 $h^{-1}$) |
|---|---|---|---|---|
| *rhoA* | An18g05980 | 9.40 ± 1.06 | 11.10 ± 0.72 | 10.00 ± 0.62 |
| *rhoB* | An16g04200 | 1.61 ± 0.37 | 3.51 ± 0.30 | 3.54 ± 0.03 |
| *rhoC* | An11g09620 | 0.43 ± 0.05 | 0.41 ± 0.02 | 0.51 ± 0.02 |
| *rhoD* | An14g05530 | 0.63 ± 0.01 | 1.28 ± 0.08 | 1.69 ± 0.10 |
| *racA* | An11g10030 | 2.15 ± 0.00 | 1.58 ± 0.08 | 1.41 ± 0.16 |
| *cftA* | An02g14200 | 2.45 ± 0.33 | 1.76 ± 0.02 | 2.08 ± 0.12 |

Mean expression values are given in % compared to the expression level of the actin gene *actA*. Data is taken from three independent cultivations: **a:** (Meyer et al. 2007b), **b**:(Jørgensen et al. 2009), **c**. (Jørgensen et al. 2010).

protein (Fig. S1). We thus designated the respective ORFs *rhoA*, *rhoB*, *rhoC*, *rhoD*, *racA* and *cftA* (cdc forty two), respectively.

To evaluate expression of these six predicted GTPase-encoding genes, we examined Affymetrix gene arrays obtained from young germlings (Meyer et al. 2007b), from exponentially growing cultures (Jørgensen et al. 2010) and from carbon-limited chemostat cultivations (Jørgensen et al. 2009). When compared to the expression of the actin gene *actA*, all Rho GTPase-encoding genes are rather moderately expressed (Table 1). When compared among each other, *rhoA* displays highest and *rhoC* lowest transcript levels.

## Individual Rho GTPase executes distinct functions

To study the roles of the Rho GTPases in *A. niger*, respective deletion mutants were generated by employing recently described protocols (Carvalho et al. 2010; Meyer et al. 2010b). All genes but *cftA* were deleted in strain MA70.15 (Δ*ku70*, *pyrG*$^{-}$) using the *A. oryzae pyrG* gene as selection marker, *cftA* was deleted in strain MA78.6 (Δ*ku70*) via hygromycin selection. We were able to obtain viable deletion mutants for five GTPases (hereafter referred to as Δ*rhoB*, Δ*rhoC*, Δ*rhoD*, Δ*racA*, Δ*cftA,* Table 2); however, deletion of *rhoA* caused a lethal phenotype. Primary Δ*rhoA* transformants were only cultivable as heterokaryons containing nuclei with the genotype *rhoA/pyrG*$^{-}$ and nuclei with the genotype *ΔrhoA/pyrG*$^{+}$ (data not shown). Deletion of the different Rho-related GTPases as well as the heterokaryotic status of *rhoA* transformants was verified by Southern analysis (data not shown) and by RT-PCR (Fig. 1).

**Table 2.** Strains used in this work.

| Strain | Relevant genotype | Source |
|---|---|---|
| *A. niger* | | |
| N402 | wild-type | Lab collection |
| AB4.1 | *pyrG*$^{-}$ | (van Hartingsveldt et al. 1987) |
| AO4.13 | *pyrG*$^{+}$(derivative of AB4.1 containing *A. oryzae pyrG*) | This work |
| MA70.15 | *ΔkusA, pyrG*$^{-}$ (derivative of AB4.1) | (Meyer et al. 2007a) |
| MA78.6 | *ΔkusA, pyrG*$^{+}$(derivative of MA70.15 containing *A. niger pyrG*) | (Carvalho et al. 2010) |
| MK11.4 | Heterokaryon *ΔkusA, rhoA/pyrG*$^{-}$*, ΔrhoA/pyrG*$^{+}$ | This work |
| ER2.5 | *ΔkusA, ΔrhoB::AopyrG* | This work |
| ER3.4 | *ΔkusA, ΔrhoC::AopyrG* | This work |
| ER7.6 | *ΔkusA, ΔrhoD::AopyrG* | This work |
| MA80.1 | *ΔkusA, ΔracA::AopyrG* | This work |
| MA84.1 | *ΔkusA, ΔcftA::hygR* | This work |
| MA80.1.1 | *ΔkusA, ΔracA, pyrG*$^{-}$ (derivative of MA80.1) | This work |
| MK3.5 | *ΔkusA, ΔracA, PinuE::racA* (derivative of MA80.1.1) | This work |
| MK4.1 | *ΔkusA, ΔracA, PinuE::racA, ΔcftA::hygR* (derivative of MK3.5) | This work |
| MK9.4 | *ΔkusA, ecfp::tubA* (derivative of MA70.15) | This work |
| MK10.2 | *ΔkusA, ΔracA, ecfp::tubA* (derivative of MA80.1.1) | This work |
| EB6.3.1 | *ΔkusA, ΔracA, egfp::racA* (derivative of MA70.15) | This work |
| MA61.24 | *PinuE::racAG18V* (derivative of AB4.1) | This work |
| MA1.8 | *PglaA::racA* (derivative of AB4.1) | This work |
| MA60.15 | *PglaA::racAG18V* (derivative of AB4.1) | This work |
| MA75.2 | *ΔkusA, ΔriaA::AopyrG* | This work |
| MA76.1 | *ΔkusA, ΔriaB::AopyrG* | This work |
| MA82.2 | *ΔkusA, ΔnoxA::AopyrG* | This work |
| *S. cerevisiae* | | |
| MAV203 | *MATα; leu2-3,112; trp1-901; his3Δ200; ade2-101; cyh2R; can1R; gal4Δ; gal80Δ; GAL1::lacZ; HIS3*$_{UASGAL1}$*::HIS3@LYS2; SPAL10* $_{UASGAL1}$*::URA3* | Invitrogen |
| MAsc1 | MAV203; pDEST32-racA; pDEST22-riaA | This work |
| MAsc2 | MAV203; pDEST32-racA; pDEST22-riaB | This work |
| MAsc3 | MAV203; pDEST32-racA; pDEST22 | This work |
| MAsc4 | MAV203; pDEST32-racA$^{G18V}$; pDEST22-riaA | This work |
| MAsc5 | MAV203; pDEST32-racA$^{G18V}$; pDEST22-riaB | This work |
| MAsc6 | MAV203; pDEST32-racA$^{G18V}$; pDEST22 | This work |
| MAsc7 | MAV203; pDEST32-racA$^{D124A}$; pDEST22-riaA | This work |
| MAsc8 | MAV203; pDEST32-racA$^{D124A}$; pDEST22-riaB | This work |
| MAsc9 | MAV203; pDEST32-racA$^{D124A}$; pDEST22 | This work |
| MAsc10 | MAV203; pDEST32-cftA; pDEST22-riaA | This work |
| MAsc11 | MAV203; pDEST32-cftA; pDEST22-riaB | This work |
| MAsc12 | MAV203; pDEST32-cftA; pDEST22 | This work |
| MAsc13 | MAV203; pDEST32-cftA$^{G14V}$; pDEST22-riaA | This work |
| MAsc14 | MAV203; pDEST32-cftA$^{G14V}$; pDEST22-riaB | This work |
| MAsc15 | MAV203; pDEST32-cftA$^{G14V}$; pDEST22 | This work |
| MAsc16 | MAV203; pDEST32-cftA$^{D120A}$; pDEST22-riaA | This work |
| MAsc17 | MAV203; pDEST32-cftA$^{D120A}$; pDEST22-riaB | This work |
| MAsc18 | MAV203; pDEST32-cftA$^{D120A}$; pDEST22 | This work |

We analyzed the phenotypes of the deletion strains on complete and minimal medium (MM) using the following descriptors: germination rate, hyphal morphology, septum formation, radial growth rate, sporulation efficiency and cell wall integrity (see *Experimental procedures* and Fig. 2). The terminal phenotype of the Δ*rhoA* heterokaryotic mutant was characterized by swollen spores, only a very few of which (less than 0.5%) developed into malformed germlings before stopped growing (data not shown). This suggests that RhoA is not *per se* important for the process of spore swelling but already indispensable for early events during germ tube formation.

As summarized in Fig. 2, the Δ*rhoB* strain was indistinguishable from the wild-type (wt) strain in terms of hyphal morphology, septum formation and radial growth rate but displayed a slightly reduced germination rate (89% of the wt rate). However, main differences were observed in terms of sporulation efficiency (about 50% fewer spores were produced by Δ*rhoB*), implicating that RhoB is important for sustaining efficient sporulation. Moreover, Δ*rhoB* was hypersensitive to the cell wall disrupting agent calcofluor white (CFW). Hypersensitivity to this compound is a reflection of defects in the biosynthesis and assembly of cell wall polymers, mainly chitin and glucans (Ram et al. 2004; Ram and Klis 2006). The reduced resistance of Δ*rhoB* would thus suggest a potential role of RhoB in cell wall deposition and integrity, a hypothetic role that would be in agreement with the function of the *S. pombe* orthologous Rho2 protein in α-1,3 glucan synthesis and cell wall integrity signaling (Calonge et al. 2000; Perez and Rincon 2010).

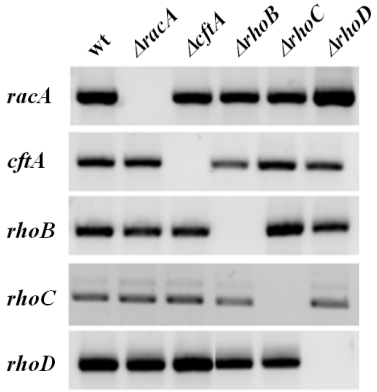


**Fig. 1**. RT-PCR of total RNA purified from different *A. niger* strains.
Wild-type and deletion strains were cultivated in liquid CM. Specific primer pairs were used to amplify Rho GTPase genes. The absence of a signal confirms successful deletion of a locus.

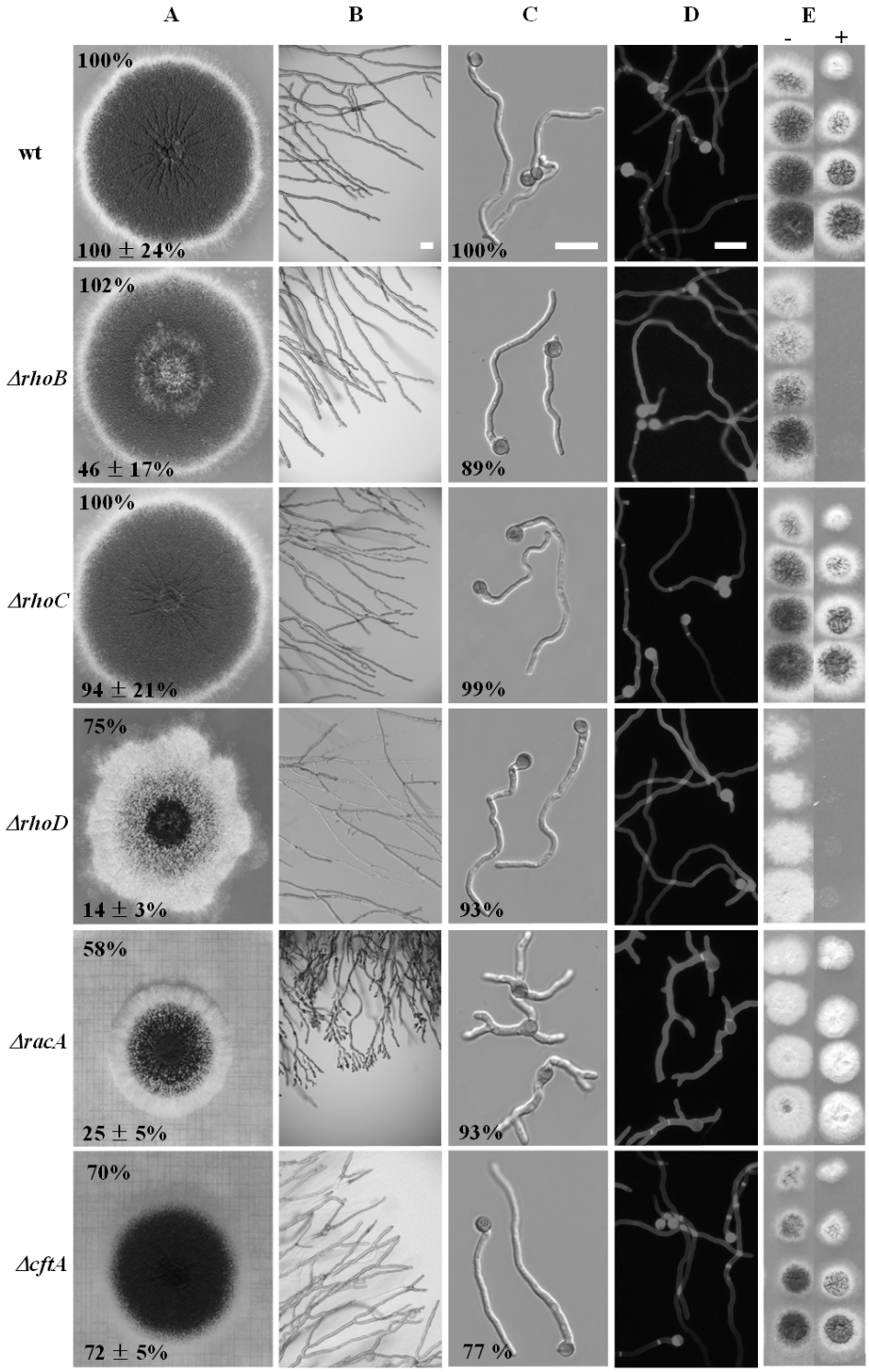
A
B
C
D
E
-
+
wt
100%
100 ± 24%
100%
ΔrhoB
102%
46 ± 17%
89%
ΔrhoC
100%
94 ± 21%
99%
ΔrhoD
75%
14 ± 3%
93%
ΔracA
58%
25 ± 5%
93%
ΔcftA
70%
72 ± 5%
77 %

**Fig. 2**. Macroscopic and microscopic phenotypes of individual Rho GTPase deletion strains. Column **A**: $10^5$ spores were point inoculated on CM agar plates and incubated for 4 days at 30°C. The macroscopic phenotypes for the different mutants were essentially the same on MM plates (data not shown). Number in the upper left of each panel reflects relative colony growth rate, number in the lower left depicts relative sporulation rate (spores/$cm^2$) compared with the wt strain MA78.6. Mean values of a triplicate experiment are given. Column **B**: Microscopic pictures with a 65x magnification from the colony edges on CM agar. Bar, 50 µm. Column **C**: Spores were allowed to germinate for 10 h at 30°C on cover slips in MM. Microscopic pictures were taken with a 200x magnification. Number in the lower left depicts the % of germinated spores (n > 150). Bar, 20 µm. Column **D**: Germlings were fixed and stained with CFW. The presence or absence of the first septum localized next to the spore was scored (n > 40). Bar, 20 µm. Higher magnification imagess of wt and Δ*rhoD* are shown in Fig. S2. Column **E**: Serial spore dilutions were spotted on MES-buffered CM (pH 6.0) containing 0 (-) or 100 µg/ml CFW (+). Colony pictures were taken after cultivation for 2 days at 30°C.

Deletion of *rhoC* did not have any obvious consequences for *A. niger*, suggesting that the cellular role of RhoC is rather negligible. This phenotype is completely different from the almost lethal *RHO3* deletion phenotype described for *S. cerevisiae* (Matsui and Toh-e 1992).

In the case of Δ*rhoD*, radial growth rate was reduced compared with its parental strain (75%; Fig. 2). Moreover, septum formation, as detected by CFW staining, was almost absent in the Δ*rhoD* strain, a phenotype that exactly resembles the Δ*rho4* phenotype observed for *N. crassa* and *A. nidulans* (Rasmussen and Glass 2005; Si et al. 2010). Close microscopic examination of Δ*rhoD* hyphae revealed that many of them were empty. Such a lysing phenotype could suggest that RhoD is important for cell wall biosynthesis in *A. niger*. In such a case, one would expect a hypersensitive phenotype of Δ*rhoD* towards CFW, which was indeed the case (Fig. 2). Finally, the Δ*rhoD* strain was strongly inhibited in sporulation as the amount of conidia produced was decreased to almost 10%. Such a reduction in conidiation efficiency has previously been associated with defects in septum formation in *A. nidulans* (Harris et al. 1994).

Pleiotropic effects were caused when *A. niger* was deleted for *racA*. Spores lacking *racA* frequently developed two or three equally long germ tubes, although formation of the second germ tube is in general delayed in wt spores (Fig. 2 and Table 3). As Δ*racA* spores simultaneously established multiple polarity axes might suggest that RacA has functions in timing axis formation and/or in stabilizing established polarity axes. In consequence, the Δ*racA* strain displayed a hyperbranching phenotype (caused by dichotomous branching) and formed a compact colony which was reduced in its diameter. In general, germ tubes and hyphae had a wider hyphal diameter in the Δ*racA* strain. Furthermore, deletion of *racA* considerably compromised conidiospore formation – only 25% conidiospores were produced compared with the wild-type.

**Table 3**. Growth-related characteristics of different *A. niger* wild type and deletion strains.

| Strain | Relevant Genotype | Germination[a] [%] | | | | Radial growth rate[b] [%] | Sporulation[b] [%] |
|---|---|---|---|---|---|---|---|
| | | N = 0 | N = 1 | N = 2 | N = 3 | | |
| MA78.6 | wt | 3.0 | 67.7 | 29.3 | 0.0 | 100.0 ± 2.0 | 100.0 ± 28.8 |
| MA80.1 | *ΔracA* | 4.9 | 46.7 | 45.7 | 2.7 | 63.1 ± 1.4 | 24.0 ± 11.8 |
| MA84.1 | *ΔcftA* | 18.8 | 81.2 | 0.0 | 0.0 | 69.7 ± 1.4 | 36.3 ± 3.2 |
| MA75.2 | *ΔriaA* | 0.0 | 73.4 | 26.6 | 0.0 | 103.3 ± 2.5 | 53.3 ± 4.0 |
| MA76.1 | *ΔnoxA* | 1.0 | 62.6 | 36.4 | 0.0 | 104.9 ± 1.4 | 48.6 ± 2.7 |
| MA82.2 | *ΔriaB* | 28.6 | 56.8 | 14.6 | 0.0 | 91.8 ± 1.4 | 84.5 ± 11.7 |

**a**: $1\times10^5$ spores were inoculated per ml liquid CM and incubated for 7 h at 37°C. The amount of germinated and non-germinated spores were counted (n > 150) and expressed in %. N = number of germ tubes formed. N = 0: % of non-germinated spores, N ≥ 1: % of spores with one or more germ tubes. **b:** $1\times10^5$ spores were point-inoculated on CM agar plates and incubated for 3 days at 30°C. The colony diameter and the amount of spores formed per $cm^2$ colony were determined and expressed in %.

To our surprise, deletion of *cftA* only mildly perturbed growth of *A. niger* and did not resemble the *A. nidulans* Δ*cdc42* phenotype (Virag et al. 2007). Basically, germ tube formation was delayed and reduced in Δ*cftA* (77% compared with wild-type) as was the growth rate (70%) and sporulation efficiency (72%; Fig. 2 and Table 3). Also, hyphal morphology remained unaffected, which could suggest that CftA has apparently no role in hyphal morphogenesis. In order to confirm that the deletion phenotypes observed were indeed caused by non-functional Rho genes, the Δ*rhoB*, Δ*rhoD*, Δ*racA*, Δ*cftA* strains were retransformed with functional gene copies. In all cases, the wt phenotype became restored back after reintroducing the respective Rho gene (Fig. S3).

## RacA and CftA share overlapping functions

The closest homolog of RacA in the yeasts *S. cerevisiae* and *S. pombe* is Cdc42p, which is an essential protein for both organisms (Johnson and Pringle 1990; Miller and Johnson 1994). One explanation why RacA or CftA is not essential for *A. niger* might be that both proteins have related functions which are executed in yeast only by Cdc42p. Hence, deletion of one protein in *A. niger* might be compensated by the presence of the other. Such an allocation of cellular tasks has recently been described for RacA and ModA (Cdc42) in *A. nidulans* (Virag et al. 2007). To examine whether this scenario is also valid for *A. niger*, we followed two genetic approaches. First, we transformed the Δ*racA* strain with the *cftA*

deletion construct. None of the primary transformants obtained yielded in any viable homokaryotic double deletion mutant on uridine-deplete medium (Δ*racA*) supplemented with hygromycin (Δ*cftA*), implying that loss-of-function mutations in both genes are synthetically lethal (data not shown).

In the second approach, we aimed to express *racA* under control of an inducible promoter in a Δ*cftA*Δ*racA* background strain. In doing so, we constructed an expression cassette, where *racA* gene expression is under control of the *inuE* promoter, and transformed it into the Δ*racA* strain, which was made *pyrG*$^{-}$ using 5'-fluoroorotic acid (FOA) counter selection (see *Experimental procedures*, Fig. 3). The *inuE* promoter itself is a strongly inducible promoter in the presence of sucrose but repressed by glucose (Yuan et al. 2008a). We confirmed that P*inuE*-driven *racA* expression rescued the multi-germination phenotype of Δ*racA* mutant on sucrose medium (Fig. 3C) but not on glucose medium (Fig. 3D). In general, P*inuE*-driven (over)expression of *racA* did not have any negative impact on hyphal morphology. This strain (P*inuE*::*racA*, Δ*racA*) was eventually used as a recipient strain to delete *cftA*. Transformants were selected and purified on uridine-deplete sucrose medium (P*inuE*::*racA* expression) supplemented with hygromycin (Δ*cftA*). Southern analysis on selected transformants confirmed that these strains were homokaryons successfully deleted for both *racA* and *cftA* (data not shown). Spore germination and morphology of these strains (P*inuE*::*racA*; Δ*racA;* Δ*cftA*) were completely rescued on sucrose medium but not on glucose medium (Fig. 3E-F), which demonstrated that RacA is capable of substituting for CftA, thereby implying that both proteins share at least one function required for polarity establishment/maintenance. Notably, the malformed germlings phenotype observed in glucose medium (Fig. 3F) is reminiscent of the phenotype observed for the *A. nidulans* fimbrin deletion mutant (Upadhyay and Shaw 2008) and in general resembles the phenotype of *A. nidulans* and *A. niger* wt germlings when treated with cytochalasin A ((Taheri-Talesh et al. 2008) and ourown unpublished observations). As cytochalasin A blocks polymerization of actin at its barbed end (Cooper 1987), we suspected that one overlapping function of CftA and RacA might be related to the elongation of actin filaments.

## RacA is important for actin but not tubulin organization

RacA appeared to be the most critical Rho GTPase important for maintaining hyphal polarity in *A. niger*. We thus focused our research interest on RacA to specifically learn more about its contribution to hyphal morphogenesis of *A. niger*. As discussed above, one function of RacA might probably be linked to the actin cytoskeleton – as also documented

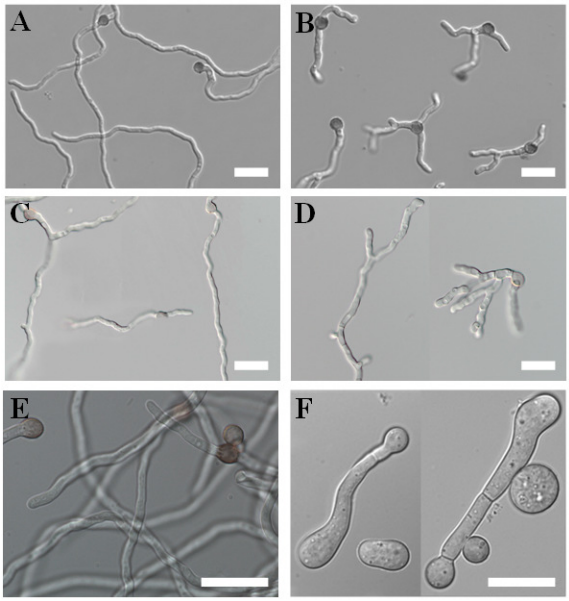


**Fig. 3.** Conditional expression of the *racA* gene (P*inuE*::*racA*) in a Δ*racA* and Δ*racA*Δ*cftA* genetic background. Spores of the different strains were allowed to germinate for 16 h at 25°C in MM. A, wt (strain MA78.6). B, Δ*racA* (strain MA80.1). C, Δ*racA* transformed with P*inuE*::*racA* (strain MK3.5) in MM containing sucrose as carbon source. D, Δ*racA* transformed with P*inuE*::*racA* (strain MK3.5) in MM containing glucose as carbon source. E, Δ*racA*Δ*cftA* strain transformed with P*inuE*::*racA* (strain MK4.1) in MM containing sucrose as carbon source. F, Δ*racA*Δ*cftA* strain transformed with P*inuE*::*racA* (strain MK4.1) in MM containing glucose as carbon source. Bar, 20 µm. Note: the *inuE* promoter is not completely tight under non-inducing condition (glucose). Its residual activity thus allows spores to germinate.

for RacA orthologs in higher eukaryotes (Bosco et al. 2009). To substantiate that presumption, we immunolabelled actin in the wt strain and in Δ*racA*. As shown in Fig. 4, actin signals are evenly distributed at cortical spots throughout wt hyphae and are concentrated near hyphal apices (Fig. 4), an actin distribution pattern that has also been described for *A. nidulans* (Harris et al. 1994). However, in the Δ*racA* strain, actin was hyperpolarized at the hyphal tip and moreover, the amount of actin in the subapical/lateral regions was reduced (Fig. 4), indicating that RacA controls actin polarization.

We also examined the consequences of a *racA* null mutation on the organization of the microtubule cytoskeleton and expressed for this purpose an CFP::TubA fusion protein in both the wt and the Δ*racA* strain. We could, however, not observe any remarkable differences in microtubule formation and localization between both strains (Fig. 4 and

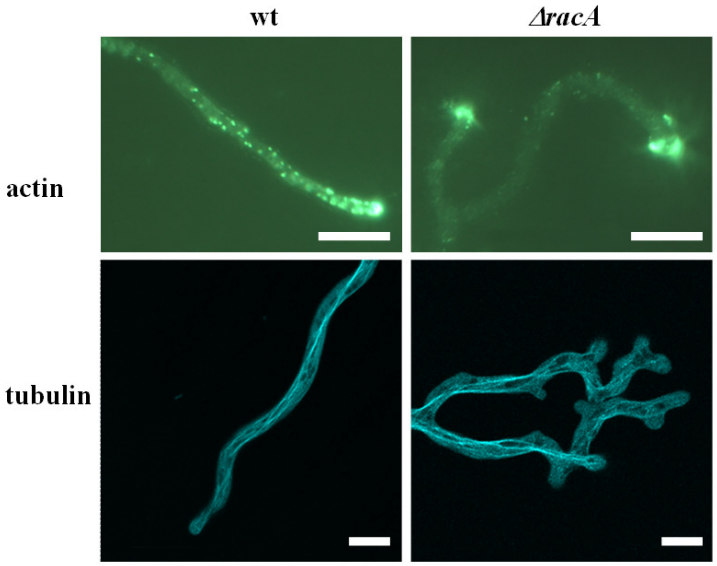


**Fig. 4.** Actin and tubulin localization in wt and Δ*racA* strain.
Actin was immunostained in strain MA78.6 (wt) and MA80.1 (Δ*racA*). Spores were cultivated on cover slips for 20 h at 25°C in MM. After cell fixation and cell wall digestion, samples were immunolabelled and analyzed by fluorescence microscopy. Tubulin (CFP::TubA) was visualized by fluorescence microscopy in strains MK9.4 (wt) and MK10.2 (Δ*racA*). Life-images were taken from cultures grown for 2 days at 20°C on MM agar. Bar, 10 µm.

data not shown). In addition, the Δ*racA* strain did not exhibited any increased sensitivity to microtubule inhibitors benomyl and nocodazole (data not shown), altogether suggesting that RacA controls actin dynamics at the hyphal tip but plays a minor if any role in microtubule organization.

## RacA localizes to the hyphal apex and ensures polarized tip growth

The data described above strongly indicated that the *A. niger* RacA secures hyphal tip growth via controlling the actin cytoskeleton. This however, is suggestive of a mainly tip-localized distribution of RacA. To test this prediction, we generated an expression construct *gfp::racA*, which we targeted to the *racA* genomic locus in such a way that the endogenous *racA* gene became replaced by the fusion construct and *gfp::racA* expressed under control of the endogenous *racA* promoter. Comparison of the phenotypes of wt, Δ*racA* and GFP::RacA strains uncovered that expression of GFP::RacA was not fully able to

complement the deletion phenotype of the Δ*racA* strain (Fig. 5A), suggesting that the GFP::RacA fusion protein was only partially functional. However, GFP::RacA was strongly polarized at the apex of germinating cells and mature hyphae and displayed a crescent-like form (Fig. 5B). Remarkably, GFP::RacA localized at hyphal apices only in actively growing cells. The signal immediately disappeared when cells stopped growing but reappeared when growth was resumed (Movie S1 and data not shown). Very rarely, we also noticed some GFP::RacA fluorescence at septa or sites destined for septum formation.

To further elucidate the role of RacA in the control of cell polarity, we wished to study the effects of *racA* overexpression on hyphal tip growth. Induced overexpression of RacA by the *inuE* promoter did not interfere with polarized tip growth (see above), pointing to the possibility that the activity of a RacA-GAP might be sufficient to inactivate RacA. We thus generated a dominant active allele of RacA, which carries the GTPase-negative G12V mutation (G18V in RacA) in the predicted GTP binding and hydrolysis domain. This mutation has been shown to trap Rho GTPases in their "on-state" (Warne et al. 1993; Ziman et al. 1991). Expression of $racA^{G18V}$ was put under control of the *inuE* promoter (sucrose-inducible, high activity during germination) or the *glaA* promoter (induced by maltose, repressed by xylose; high activity during exponential growth phase) and the three constructs generated (P*glaA*::*racA*, P*glaA*::$racA^{G18V}$, P*inuE*::$racA^{G18V}$) were targeted to the *pyrG* locus of *A. niger*. As shown in Fig. 6, P*inuE* – driven expression of $RacA^{G18V}$ resulted in the formation of clavate-shaped germlings which were abnormally large, unpolarized and

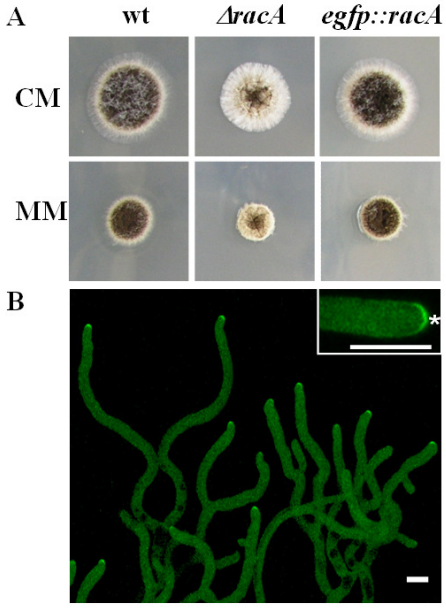


Fig. 5. RacA localization in growing hyphae of *A. niger*.
A, Colony pictures of wt (MA78.6), Δ*racA* (MA80.1) and GFP::RacA (EB6.3.1) on CM agar. B, Life-images of the GFP::RacA strain were taken from cultures grown for 2 days at 25°C on MM agar. The cap-like distribution of GFP::RacA is indicated with a star. Bar, 10 µm.

contained extremely large vacuoles (Fig. 6A and B). When expression of *racA*$^{G18V}$ was under control of the *glaA* promoter, hyphae showed a pronounced swollen-tip phenotype and formed bulbous lateral branches (Fig. 6D and F). Thus, both strains expressing constitutive active RacA$^{G18V}$ are defective in tip elongation, indicating that controlling RacA activity is inevitable for polarity maintenance. To test whether this loss of polarity might be a consequence of disturbed actin localization, we immunolabelled actin in the P*glaA*::*racA*$^{G18V}$ and P*inuE*::*racA*$^{G18V}$ strains. As depicted in Fig. 7, actin polarization was indeed lost in both strains and actin signals were randomly scattered intracellularly or at the cell periphery.

## RacA interacts with a protein of unknown function and with NoxR

In order to identify potential downstream effectors of RacA, a yeast two-hybrid screen was

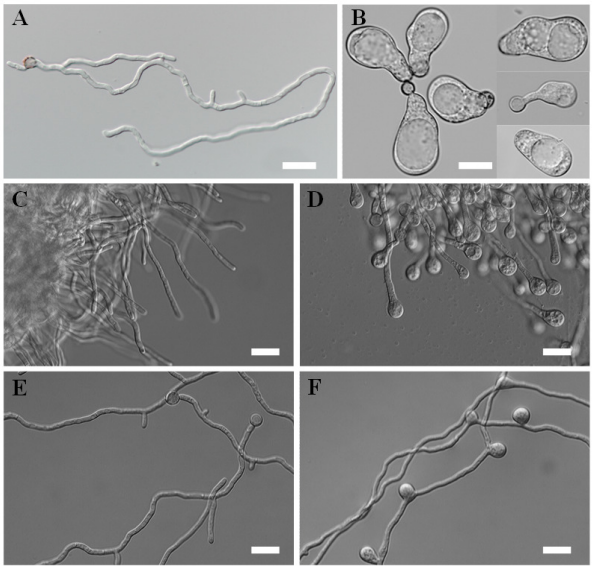


**Fig. 6.** Microscopic analysis of RacA$^{G18V}$ strains.
A and B, Microscopic phenotypes of wt (AO4.13) and the P*inuE*::*racA*$^{G18V}$ strain MA61.24, respectively, when cultivated in MM with 1% sucrose as carbon source. C and D, Microscopic phenotypes of wt (AO4.13) and the P*glaA*::*racA*$^{G18V}$ strain (MA60.15), respectively, when cultivated in shake flasks till the mid-exponential growth phase using 2% maltose as carbon source. E and F, Microscopic phenotypes of wt (AO4.13) and the P*glaA*::*racA*$^{G18V}$ strain (MA60.15), respectively, when grown on cover slips in MM with maltose as carbon source. Bar, 20 µm.

performed using RacA$^{G18V}$ as bait and different prey libraries. The libraries used harbored mRNA populations isolated from different morphological stages of *A. niger* (germination, vegetative growth, conidiation) and from stressed mycelium (see *Experimental procedures*). Interestingly, RacA$^{G18V}$ interacting proteins (Ria) were only identified from the conidiation and the stressed cDNA library and altogether only two Ria proteins were isolated. RiaA (An16g05550) was isolated from the conidiation library and displayed strong interaction with RacA$^{G18V}$, RiaB (An12g06420) was identified from the stress library and interacted only weakly with RacA$^{G18V}$ (Fig. 8). *riaB* encodes a zinc knuckle domain protein, having no apparent homolog outside the fungal kingdom and whose function is unknown. The interaction of RiaB is, although weak in its nature, specific for RacA$^{G18V}$ as we have not detected any interaction of RiaB with RacA and RacA$^{D124A}$ nor with CftA, CftA$^{G14V}$ and CftA$^{D120A}$, suggesting that RiaB binds to RacA only when in its activated, GTP-bound form (Fig. 8, note that the D124A mutation in RacA and D120A mutation in CftA, respectively, are dominant negative (Ziman et al. 1991)).

To study the function of both RiaA and RiaB, we deleted the respective genes in *A. niger*, which was verified by Southern analysis (data not shown). Surprisingly, deletion of *riaB* did not manifest in a strong phenotype (Fig. S4A). Only germination of Δ*riaB* was delayed and the growth rate slightly reduced when compared with the wt situation (Table 3). These observations might hint at the possibility that RiaB's function and its interaction with activated RacA are necessary for securing maximal polar growth rate of *A. niger*.

The *riaA* gene codes for a protein with strong sequence similarity to the NADPH

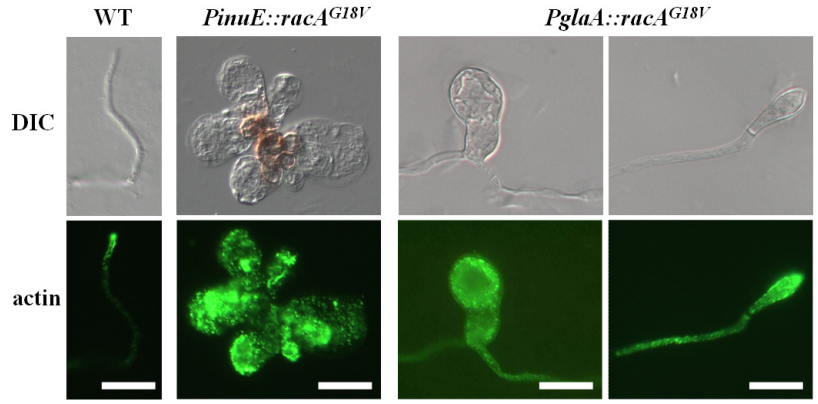


**Fig. 7.** Actin distribution in RacA$^{G18V}$ strains.
Actin staining of young hyphae from wt strain (AO4.13), strains MA61.24 (P*inuE*::*racA*$^{G18V}$) and MA60.15 (P*glaA*::*racA*$^{G18V}$) was performed as described in Fig. 4. DIC micrographs are shown for comparison.

oxidase regulator NoxR/p67$^{phox}$ (68% identity to the *A. nidulans* NoxR, 36% identity to the human p67$^{phox}$). In mammals, NADPH oxidases (Noxs) are members of a multi-protein complex to which, among others, p67$^{phox}$ and Rac1 are bound and which generate ROS (Lambeth 2004). In filamentous fungi, it was recently shown that a tip-proximal gradient of ROS is essential to sustain apical dominance and that interaction of RacA and NoxR is required to activate Nox activities (Cano-Dominguez et al. 2008; Rolke and Tudzynski 2008; Scott and Eaton 2008; Semighini and Harris 2008; Tanaka et al. 2008). Interestingly, the interaction of RiaA (NoxR) with RacA was specific for RacA but independent from its GTP/GDP status: RiaA (NoxR) interacted with RacA, RacA$^{G18V}$ and dominant negative RacA$^{D124A}$ but not with CftA, dominant active CftA$^{G14V}$ and dominant negative CftA$^{D120A}$ (Fig. 8). Unexpectedly, deletion of *riaA* as well as deletion of the predicted NoxA protein (An08g10000; *A. niger* possesses only a single *nox* gene) did not cause any morphological defects in *A. niger* (Fig. S4A, for complementation analyses of Δ*noxA* and Δ*riaA* (*noxR*), see Fig. S3). Only sporulation efficiency was reduced in Δ*riaA* and Δ*noxA* strains to about 50% (Table 3). Moreover, we could not detect any differences in the discrete tip localization of ROS using nitro blue tetrazolium (NBT) staining of wt, Δ*riaA* and Δ*noxA* hyphae (Fig. S4B), implying that an interaction of RacA with RiaA is rather important for asexual developmental processes but not for hyphal tip growth as shown for *A. nidulans* (Semighini and Harris 2008).

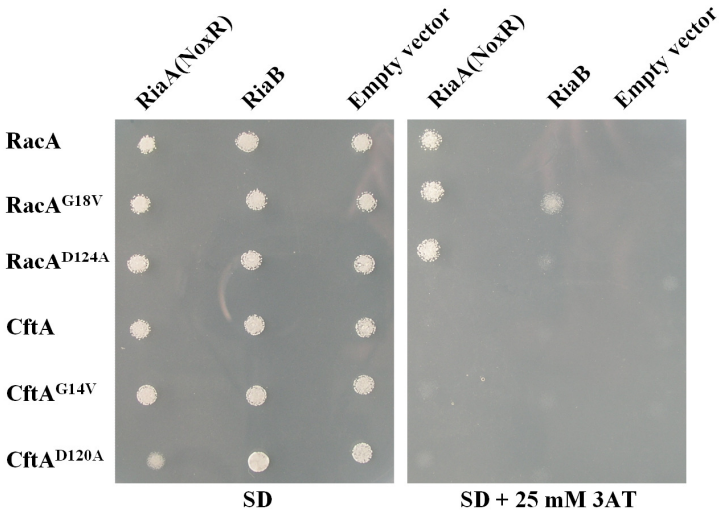


**Fig. 8.** Yeast-two hybrid interactions of RacA or CftA with RiaA and RiaB, respectively.
A total of $10^3$ yeast cells from logarithmically growing cultures were spotted on minimal medium lacking leucine, tryptophan and histidine (SD) and cultivated for 24 h at 30°C. Growth on SD + 25 mM 3-AT is indicative for a protein-protein interaction. All interactions were confirmed using *lacZ* as reporter (data not shown).

# Discussion

Rho GTPases are intracellular signalling molecules present from lower eukaryotes up to mammals but absent in eubacteria and archaea. They are key regulators of cell shape and polarity and were first described as modulators of the actin cytoskeleton (Hall 1998). Later it became evident that Rho GTPases interact not only with actin but with multiple target proteins, thus participating in many distinct processes such as metabolism, vesicular transport, proliferation, survival and even gene expression (Ridley 2001; Ridley 2006).

Recently, the ontogeny of Rho GTPases was reconstructed from major eukaryotic clades and the chronology of their emergence revisited. Basically, Rac is the founder of the Rho family, and Cdc42 and Rho1 diverged from Rac about 1.5 billion years ago. Duplications, gene loss, gene rearrangements and horizontal gene transfer of Rac, Rho1 and Cdc42 descendants finally resulted in varying repertoires of Rho family members in different eukaryotes (Boureux et al. 2007). For example, *S. cerevisiae* does not harbor a Rac homolog, Cdc42 is not present in *Arabidopsis thaliana* and *Dictyostelium discoidium* and some eukaryotes such as filamentous fungi and mammals comprise both Rac and Cdc42 proteins (Boureux et al. 2007). The evolution of Rho family members has profound consequences on their involvement in polar growth control in different model systems. Although the three hierarchical steps are the same (polar site selection by internal or external cues, establishment of the polar axis, maintenance of the polar axis coupled with polar growth), the specific GTPase(s) involved can differ and the specific mechanism that governs these steps as well. For example, the three hierarchical processes are orchestrated by three different GTPases in *S. cerevisiae* (Ras, Cdc42, Rho1) but only by a single Rac-like GTPase (Rop) in plants (Fu and Yang 2001). Within the group of filamentous Ascomycetes, the relative requirement for RacA for polar growth control differs as well ((Chen et al. 2008; Rolke and Tudzynski 2008; Virag et al. 2007) and this work).

## Rho GTPases of *A. niger* exert distinct and mutual functions

Recent advances in genomics and gene targeting tools for *A. niger* has allowed us to identify and selectively inactivate all predicted Rho GTPases in this industrial model organism thereby getting insights into their physiological roles (Figs. 2 and 3). Given the phenotypic traits of the Δ*rhoA/rhoA*, Δ*rhoB*, Δ*rhoC*, Δ*rhoD*, Δ*racA*, Δ*cftA* and Δ*racA*Δ*cftA* strains during the life cycle of *A. niger*, we propose the following model (Fig. 9): RhoA occupies a central role in controlling polarity establishment and additionally exerts functions which are essential for the viability of *A. niger*. RhoB and RhoD are important for

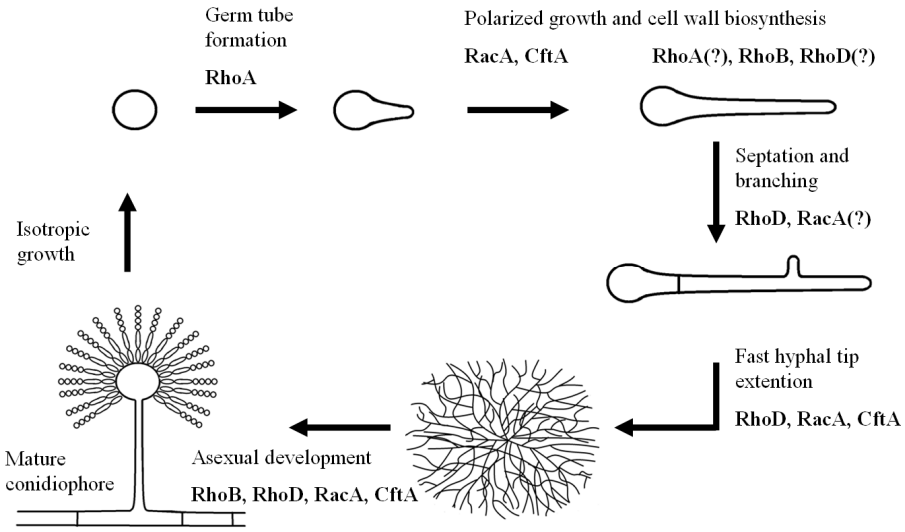


**Fig. 9.** Predicted functions of different Rho GTPases during the life cycle of *A. niger* as deduced from phenotypic traits of respective loss-of-function mutations. For details see Discussion.

cell wall biosynthesis, RhoD governs cytokinesis (septation and sporulation) and RacA controls polarity maintenance, which can partially also be accomplished by CftA. Altogether, the activities of RhoD, RacA and CftA contribute to and ensure fast hyphal tip growth rate in *A. niger*.

Thus, all six Rho GTPases exert distinct and overlapping functions, which, when compared with data from other filamentous fungi, are only partially conserved. Even within a genus, there is no consistent pattern for the physiological function of Rho GTPases. For example, RhoD is required for septum formation in both *A. nidulans* and *A. niger*, but RacA and CftA differently contribute to polarity maintenance in both species ((Si et al. 2010; Virag et al. 2007) and this work). Similar and differing requirements of Rho GTPases for growth and morphogenesis of filamentous fungi are most probably a consequence of species differentiation during evolution (see above). Although fungal Rho GTPases are highly related (Fig. S1), their interaction with other molecules can differ and can cause varying species-specific outputs. Hence, studying different model systems will give comprehensive insights into the roles of Rho GTPases for fungal growth and development.

## RacA and CftA control actin dynamics in *A. niger*

The phenotypic analyses of the six different Rho GTPase deletion strains uncovered that apical dominance in young germlings and mature hyphae of *A. niger* is predominantly controlled by RacA. To understand more about the underlying mechanisms of RacA activity, we visualized RacA by GFP tagging, studied the cellular consequences of dominant activation of RacA ($RacA^{G18V}$), followed actin and tubulin distribution in wt, Δ*racA* and $RacA^{G18V}$ strains and generated a conditional Δ*racA*Δ*cftA* double deletion strain. The data shows that RacA localizes to the apex of actively growing cells, where it seems to be crucial for the organization of actin distribution (Figs. 4, 5 and 7; Movie S1). Both deletion and dominant activation of RacA provoke an actin localization defect and thereby loss of polarized tip extension (Figs. 5 and 7). In the case of RacA deletion, actin becomes hyperpolarized, whereas constitutive active RacA causes actin depolarization. Interestingly, the dichotomous branching phenotype of Δ*racA* suggests that loss of apical dominance can easily be overcome by the establishment of two new sites of polarized growth. This phenotype is reminiscent of the *ramosa-1* mutant of *A. niger*, which results from a transient contraction of the actin cytoskeleton and thereby transient displacement of the Spitzenkörper (Meyer et al. 2009; Reynaga-Pena and Bartnicki-Garcia 1997; Reynaga-Pena and Bartnicki-Garcia 2005). Frequent dichotomous branching is also a characteristic of the actin (*act*$^{1}$) and actinin mutants in *N. crassa* and *A. nidulans* (Virag and Griffiths 2004; Wang et al. 2009) as well as of the *A. nidulans* Δ*sepA* mutant (Harris et al. 1994), which would be in agreement with the concept that RacA is important to stabilize polarity axes via controlling actin. When RacA is trapped in its active, GTP-bound form ($RacA^{G18V}$), however, loss of apical dominance can not be overcome by *A. niger*. Imaginable is a mechanism similar to the control circuit shown for plant pollen tubes (Klahre and Kost 2006): A hypothetical, subapically localized, RacA-dependent GAP ensures that the activity of RacA is spatially restricted to the hyphal apex thereby maintaining a stable polarity axes. In the $RacA^{G18V}$ mutant strain, however, this hypothetical control mechanism is leveraged off.

Our data also showed that RacA can substitute for CftA (Fig. 3) and that deletion of both genes is lethal to *A. niger*, whereas deletion of each single gene is not (Fig. 2). These observations suggest that RacA and CftA share functions with respect to the control of the actin cytoskeleton. Basically, Rac1 and Cdc42 of higher eukaryotes can affect actin dynamics by three ways: They induce polymerization and branching of actin filaments by stimulating the Arp2/3 complex and formins. They support actin polymerization by activating WASP/WAVE proteins which prevent capping of the barbed (plus) end of actin filaments. And thirdly, they inhibit the actin depolymerizing factor cofilin, thereby controlling the disassembly of actin filaments at the minus end. Hence, Rac1 and Cdc42 govern actin dynamics by adjusting the assembly and disassembly rates of actin filaments

(for details see recent reviews (Heasman and Ridley 2008; Ridley 2006)). The actin hyperpolarization phenotype of the Δ*racA* strain could imply that actin turnover rates are disturbed in this strain, i.e. actin filaments disassemble too quickly. If so, it would follow that RacA and CftA can substitute each other with respect to actin polymerization but that actin depolymerization is mainly under control of RacA (Fig. 10). As a result, a *racA* deletion mutant will not be affected in actin polymerization (because secured by CftA) but will be disturbed in actin depolymerization and thus apical dominance. In contrast, a *cftA* deletion mutant is not affected in both actin polymerization and actin depolymerization as both processes can be guaranteed by RacA. Hence a *cftA* deletion strain will not be affected in the maintenance of polar tip growth, which indeed is the case (Fig. 2).

## RiaA and RiaB are downstream targets of RacA

We finally showed that RacA physically interacts with two proteins, namely RiaA, which is a predicted NoxR homolog, and RiaB, a protein of unknown function. As both proteins do not interact with CftA (Fig. 7), we suspect that they are specific downstream targets of RacA (Fig. 10). Loss-of-function analyses of RiaB showed that this protein rather fulfils a moderate physiological role and apparently ensures optimal tip extension rate (Table 3).

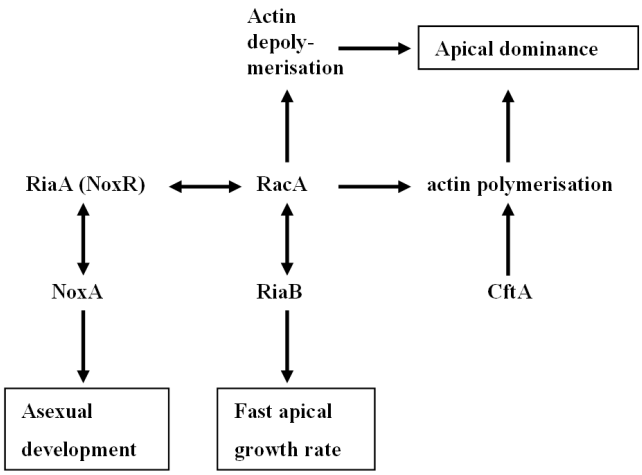


**Fig. 10.** Tentative mechanistic model explaining the function of RacA and CftA for growth, morphogenesis and development of *A. niger*. RacA interaction with effector proteins are indicated with double arrows. For details see Discussion.

As RacA interacted with RiaA, we also analyzed the consequences of *riaA* and *noxA* deletion for *A. niger*. A requirement of NoxA/NoxR proteins in hyphal tip extension and (a)sexual reproduction has been reported for different fungal species (Cano-Dominguez et al. 2008; Lara-Ortiz et al. 2003; Malagnac et al. 2004; Scott and Eaton 2008; Semighini and Harris 2008). Our phenotypic analyses of Δ*riaA* and Δ*noxA* strains strongly imply that an involvement of RiaA (NoxR) and NoxA in tip-localized ROS generation is rather unlikely in *A. niger* (Fig. S4). Although the well-developed ROS gradient towards hyphal apices still suggests that regulated synthesis of ROS is important for hyphal tip growth of *A. niger* hyphae, we propose that this is not mediated by NoxA and RiaA (NoxR). Several observations support this reasoning. First, the Δ*noxA* and Δ*riaA* strains do not display any polarity defects. Second, radial growth rate is not affected in *A. niger* when deleted for Δ*noxA* or Δ*riaA*. And third, ROS staining is not reduced in Δ*noxA* or Δ*riaA* strains when compared with the wt situation. As deletion of both proteins resulted in a strong reduction in conidia formation, we rather consider that NoxA and RiaA play an important role in asexual development of *A. niger*. Notably, the relative contribution of Nox proteins to these processes seems to be strongly species-dependent. For example, deletion of NoxA results in reduced conidiation in *N. crassa* (Cano-Dominguez et al. 2008) but not in *A. nidulans* (Semighini and Harris 2008). We currently undertake efforts to understand to which extent NoxA and RiaA contribute to developmental decisions in *A. niger*.

# Experimental Procedures

## Strains, culture conditions and molecular techniques

*A. niger* and *S. cerevisiae* strains used in this study are given in Table 3. *Escherichia coli* strain XL1-blue served as host for all plasmid work. General cloning procedures in *E. coli* were done according to (Sambrook and Russell 2001). *A. niger* strains were cultivated in minimal medium (MM) (Bennett and Lasure 1991) containing 1% glucose, as a carbon source (if not otherwise stated) or in complete medium (CM), consisting of MM supplemented with 1% yeast extract and 0.5% casamino acids. Then 10 mM uridine or 100 µg/ml hygromycin was added when required. Transformation of *A. niger*, selection procedures, heterokaryon rescue, genomic DNA extraction, diagnostic PCR and Southern analyses were performed using recently described protocols (Carvalho et al. 2010; Meyer et al. 2010b). The Δ*racA* strain was rendered uridine-requiring (*pyrG*$^{-}$) using FOA counter selection (Meyer et al. 2010b). Sensitivity of *A. niger* strains towards CFW was tested using the protocol according to (Ram and Klis 2006). The effect of the microtubule inhibitors

benomyl and nocodazole on the growth of *A. niger* strains was tested using different concentrations up to 0.25 µg/ml.

## Phenotypic analyses and staining procedures

Defined spore titres of *A. niger* strains were used to inoculated MM or CM and incubated for 1-4 days at 25-30°C. All quantitative measurements (growth rate, germination rate, sporulation efficiency) were performed in triplicates. To determine the amount of spores produced by a colony, all spores formed were carefully taken off with physiological salt solution and a cotton stick and counted using a Neubauer chamber.

Actin immunostaining, CFW and NBT staining were performed according to (Meyer et al. 2009; Meyer et al. 2008). For actin immunostaining, cells were fixed with a PBS buffer containing 3.7% p-formaldehyde, 5% DMSO, 25 mM EGTA pH 7.0 and 5 mM $MgSO_4$. Cell walls were digested for 60 min using lysing enzyme from *Trichoderma harzianum* (Sigma-Aldrich). The monoclonal antibody against actin was obtained from MP Biomedicals. For CFW staining, germlings were fixed in PBS buffer containing 3.7% p-formaldehyde and 0.2% Triton X-100, rinsed with PBS buffer and incubated in 10 µg/ml of Fluorescent Brightener 28 (CFW, Sigma-Aldrich) for 5 min after which they were rinsed again and subjected to microscopy. For NBT staining, germlings were incubated for 1 hour in 50 mM sodium phosphate buffer containing 0.5 mg/ml NBT (Sigma-Aldrich), washed once with 100% methanol and once with water and immediately subjected to microscopy.

## Microscopy

Light and fluorescence microscopic pictures were captured with 20x or 40x objectives and using an Axioplan 2 (Zeiss) equipped with a DKC-5000 digital camera (Sony). DIC and GFP settings were used and images were processed using Adobe Photoshop 6.0 (Adobe Systems).

For time-lapse microscopy, conidia were pre-grown on MM agar plate at 30°C for 2 days. An agar piece containing mycelium was transferred upside down onto an objective glass. To prevent drying-out of the agar, a small volume of CM was applied between the colony and the objective glass. After cells resumed growth, time-lapse images were captured with 40x C-apochromatic objective on an inverted LSM 5 microscope equipped with a laser scanning-disk confocal system (Zeiss). In total, eleven z stacks (0.6 µm interval) were taken in 30 s time intervals. The time-lapse movie showing 4 frames per second was assembled using ZEN 2009 software (Zeiss).

## Construction of deletion cassettes, mutant alleles and expression cassettes

Standard PCR and cloning procedures were used for the generation of all constructs (Sambrook and Russell 2001) and all cloned fragments were confirmed by DNA sequencing. Details on cloning protocols and primers used can be requested from the authors.

The *rhoA*, *rhoB*, *rhoC*, *rhoD, racA, cftA, riaA, riaB* and *noxA* deletion constructs were made by PCR amplification of the 5'- and 3'- flanks of the respective ORFs (at least 0.9 kb long). Genomic DNA of *A. niger* served as template DNA. The sequences were cloned upstream and downstream of the *A. oryzae pyrG* selection marker obtained from pAO4-13 (de Ruiter-Jacobs et al. 1989). In the case of *cftA*, the hygromycin resistance cassette isolated from pAN7-1 (Punt et al. 1987) was used to replace the *cftA* ORF.

The *PglaA::racA::TtrpC-pyrG** construct was made based on pAN52-7 (Verdoes et al. 1994a) which already contained *PglaA::TtrpC*. Next to this cassette, the *pyrG** allele of plasmid pAB94 (van Gorcom and van den Hondel 1988) was cloned to facilitate integration of the constructs at the endogenous *pyrG* locus of *A. niger*. Finally, the *racA* ORF was cloned downstream of *PglaA*. The *PinuE::racA::TtrpC-pyrG** construct was generated by exchanging P*glaA* with P*inuE,* which was gained by PCR amplification of the 1.5 kb *inuE* upstream region from genomic DNA.

*PtubA*::*ecfp::tubA::TtubA-pyrG** was generated using a fusion PCR approach recently described (Meyer et al. 2008). *PracA*::*egfp-AopyrG-egfp::racA::TracA* was made according to (Hazan and Liu 2002). Note, N-terminal tagging of small GTPases is favoured over C-terminal tagging, as the C-terminal isoprenyl group is essential for GTPase function.

Mutant alleles of *racA* and *cftA* (encoding $RacA^{G18V}$, $RacA^{D124A}$, $CftA^{G14V}$ and $CftA^{D120A}$), were generated by PCR using primers carrying respective point mutations. The DNA fragment encoding for $RacA^{G18V}$ was used to replace the *racA* gene in *PinuE::racA::TtrpC-pyrG** and *PglaA::racA::TtrpC-pyrG**, respectively. For the yeast two-hybrid assay, wt and mutant alleles of *racA* and *cftA* were cloned into pDEST32 (Invitrogen) according to the supplier's instructions.

## Complementation analyses

Complementation cassettes were generated for the deletion strains Δ*rhoB*, Δ*rhoD,* Δ*racA,* Δ*cftA,* Δ*riaA,* Δ*riaB* and Δ*noxA*, respectively. The ORFs including 1000 bp of their up- and downstream regions were amplified by PCR using genomic DNA of *A. niger* as template. The DNA fragments gained were either integrated into an autonomously replicating pAMA-based vector (Carvalho et al. 2010) or into pAN7-1 (Punt et al. 1987) and thereafter

transformed into the individual deletion strains. For complementation analyses, the strongest deletion phenotype was selected in order to analyze whether the wt phenotype became restored.

## Construction of cDNA libraries and yeast two-hybrid analysis

Four *A. niger* cDNA libraries were constructed using the CloneMiner cDNA library construction kit from Invitrogen. Library A ('vegetative growth library') was made using pooled RNA populations isolated from liquid CM cultures harvested after 4, 6, 8, 16 and 32 h of incubation. Library B ('morphological mutant library') was constructed by pooling RNAs from the hyperbranching mutant strain *ramosa-1* ((Meyer et al. 2009); cultivated in liquid CM for 16 h at permissive and 2 h at restrictive temperature) with mRNAs isolated from the *PglaA::racA*$^{G18V}$ strain (propagated for 16 h in liquid CM). Library C ('stress library') was established using RNAs extracted from 5 hour old germlings stressed for 1 h with 2 mM DTT and stressed for 1, 2 or 4 h with 200 µg/ml CFW). Library 4 ('conidiation library') was established from a culture that was pregrown for 16 h in liquid CM and transferred to a CM agar plate covered with a polycarbonate filter. RNA from sporulating mycelia was harvested after 8 h and 27 h of incubation.

For each library, equal amount of RNA from the different condition was pooled and used for reverse transcription. Each of the cDNAs obtained was cloned into the donor vector pDONR222 (Invitrogen) to create four entry libraries (each ~ $7\times10^6$ clones, average insert size 1.4-1.7 kb). The two-hybrid libraries were constructed by transferring the libraries from pDONR222 to pDEST22 via LR reactions (Invitrogen). At least $3\times10^6$ clones were isolated for each library. The yeast two-hybrid screen (screening procedure, confirmation of positive interactors using the reporter genes *HIS3*, *URA3* and *lacZ* and respective controls) was performed according to the manufacturer's instructions (ProQuest™ Two–Hybrid System with Gateway® Technology, Invitrogen). Putative interactions of RacA and CftA versions (RacA, RacA$^{G18V}$, RacA$^{D124A}$, CftA, CftA$^{G14V}$ and CftA$^{D120A}$) with RiaA and RiaB were repeatedly analyzed using *HIS3* (3-Amino-1,2,4-triazole; 3-AT) and *lacZ* as reporters following the manufacturer's instructions.

**Acknowledgements**

The authors would like to acknowledge Benjamin Nitsche for bioinformatics support and Xiao-Lian Yuan for microscopic assistance. We are grateful to Erica Bernard and Robbert Damveld for help in cloning experiments. This project was carried out within the research

programme of the Kluyver Centre for Genomics of Industrial Fermentation which is part of the Netherlands Genomics Initiative / Netherlands Organization for Scientific Research.